applied optics

Measuring the spectral response of a division-of-focal-plane polarization imager using a grating monochromator

Erica Venkatesulu and Joseph A. Shaw*

Electrical and Computer Engineering Department and Optical Technology Center, Montana State University, P.O. Box 173515, Bozeman, Montana 59717-3515, USA
*Corresponding author: joseph.shaw@montana.edu

Received 26 January 2022; revised 18 February 2022; accepted 19 February 2022; posted 23 February 2022 (Doc. ID 454801); published 16 March 2022

Spectral characterizations are performed on imagers to obtain a relative spectral response (RSR) curve. This process often utilizes a grating monochromator with an output that changes polarization as a function of wavelength (our monochromator's degree of linear polarization was found to vary from less than 10% to more than 70%). When characterizing a polarization-sensitive imager, this introduces polarization artifacts into the RSR curve. We present a simple method to avoid these polarization artifacts for division-of-focal-plane polarization imagers by directly illuminating the camera with the monochromator output and calculating the S_0 Stokes parameter at each super pixel, then we show consistent results from this method for two division-of-focal-plane polarization imagers. We also show that ignoring the monochromator polarization results in order-of-magnitude RSR errors. The recommended method uses an iris to limit the spatial extent of the monochromator output, which was found experimentally to increase the minimum signal-to-noise ratio by more than a factor of 2.

https://doi.org/10.1364/AO.454801

1. INTRODUCTION

Recent division-of-focal-plane (DoFP) [1] sensor technology has dramatically increased polarization contrast while also reducing cost [2], so a significant increase in the use of imaging systems with these sensors can be expected for myriad applications. In turn, an increased need for characterizing imaging systems using such sensors can be expected. Spectral characterizations consist of measuring the relative spectral response (RSR), which describes the change in system response as a function of the wavelength of incident light. Grating monochromators are often used to measure the RSR of optical systems by sweeping a narrowband output across the spectral range of the system [3–7]. Other methods of performing spectral characterizations use Fourier transform spectrometers [8], tunable lasers [9,10], tunable LEDs [11], multiple spectral filters in front of broadband sources [12], and stochastic optimization algorithms operating on colored sample and diffraction images [13]. However, grating monochromators often output light that is significantly polarized, with a state of polarization that varies significantly as a function of wavelength (Fourier transform spectrometers also tend to be partially polarized [14]). This varying state of polarization creates difficulties when measuring the RSR of polarization-sensitive imagers. The polarization imagers used in this work have an intentional polarization response, but it should be noted that many optical systems have unintentional polarization responses [14–18]. One method of mitigating the polarization artifacts that would result from using a polarized monochromator to measure a polarization-sensitive system is to pass the monochromator output through an integrating sphere [19,20]. The light exiting the integrating sphere will have a negligible polarization, but this may also result in photon-starved measurements. Other possibilities, such as rotating the monochromator output polarization with an achromatic wave plate also could be used to avoid polarization artifacts, but they significantly increase the complexity of the measurement.

In this work, we present a simple method of performing a spectral characterization of a DoFP polarization imager. This type of imager has differently polarized pixels adjacent to one another, allowing for the calculation of a linear Stokes vector at each superpixel. To obtain an RSR curve for this polarization imager with a polarized monochromator, we calculated the S_0 Stokes parameter, which provided a measure of total irradiance at each superpixel that was polarization-insensitive. This enabled us to determine the RSR of the polarization imager using a grating monochromator. This paper is based on work we presented at a recent SPIE conference [21], but here we report a more complete analysis that incorporates a flat-field correction and explores the spatial nonuniformity of the monochromator output to improve our results.

2. DoFP IMAGER AND MONOCHROMATOR SYSTEMS

The imagers used in this work are DoFP polarization imagers [1] that employ Sony's recently released polarization-sensitive sensor [2]. Specifically, the two imagers used in this work were the Teledyne FLIR BFS-U3-51S5P and Lucid Vision Labs TRI050S-PC. The sensors use a polarizing filter array of nanowires placed on top of the focal plane array. Adjacent pixels have differently oriented nanowires, arranged in a configuration such that it is possible to determine the linear polarization state of incident light. This configuration is shown in Fig. 1. Specifically, the nanowires are arranged so that in a 2×2 group of pixels (referred to as a superpixel), four linear polarization states are measured. Relative to horizontal, the polarizing filter array passes light polarized at 90° for the top left pixel, 45° for the top right pixel, 0° for the bottom right pixel, and 135° for the bottom left pixel. This requires nanowires oriented orthogonally to the pass axis, i.e., at 0° relative to horizontal for the top left pixel, 135° for the top right pixel, etc. This means that with a radiometric calibration, each superpixel measures irradiance at these four linear polarization states, I_{0°, I_{45°, I_{90°, and I_{135°, in its instantaneous field of view. We can use these irradiances to calculate the linear Stokes vector at each pixel using the following three equations:

$$S_0 = I_{0^\circ} + I_{90^\circ}, \tag{1}$$

$$S_1 = I_{0^\circ} - I_{90^\circ}, \tag{2}$$

$$S_2 = I_{45^\circ} - I_{135^\circ}. \tag{3}$$

The degree of linear polarization (DoLP) and angle of polarization (AoP) of the light can be calculated from the Stokes parameters. The DoLP is given by

$$\mathrm{DoLP} = \frac{\sqrt{S_1^2 + S_2^2}}{S_0}, \tag{4}$$

and the AoP is given by

$$\mathrm{AoP} = \frac{1}{2}\arctan\frac{S_2}{S_1}. \tag{5}$$

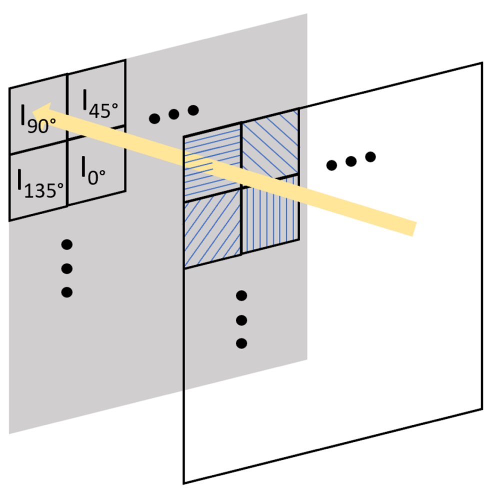

Fig. 1. Layout of a superpixel in a DoFP polarization imager. The polarizing filter array is made of nanowires oriented such that a 2×2 group of pixels can measure four linear polarization states: 0°, 45°, 90°, and 135°.

While we do not know the details of the nanowires in these commercial sensors, Sony presented a DoFP camera using wire grids with a 150-nm period (100-nm spacing and 50-nm wire width) [22]. Also, it is common for DoFP cameras to introduce a polarization bias caused by different transmissivities of differently oriented nanowires [2]. To compensate for this, as well as for random pixel-to-pixel variations, a flat-field correction was developed for both DoFP cameras at each exposure time using an integrating sphere. Without the flat-field correction, the DoFP cameras measured the integrating sphere to have a DoLP greater than 5%. We confirmed that the measured polarization was due to the camera bias rather than real polarization of the integrating sphere by rotating the camera in front of the integrating sphere and measuring the AoP. The AoP did not change as the camera angle was changed. In one previous study, a commercial integrating sphere was measured to have a degree of polarization of about 0.5% [23]. While our sphere may have a similar level of undesired polarization, this introduces a smaller error than that which would be caused by not correcting for the polarization bias of the camera. In addition, we measured the dark signal of these cameras to be approximately 1% or less and therefore did not incorporate a dark signal correction.

When using imaging systems to obtain scientifically useful data with passive remote sensing, it is often necessary to perform radiometric calibrations on the imagers. In order to perform a proper radiometric calibration of an imaging system, the RSR of the detector is multiplied by the spectral radiance of the calibration source to determine the band-integrated radiance, which is then correlated to a digital number. The requirement to know the RSR of the DoFP polarization cameras is what led us to question the polarization state of our monochromator output.

A grating monochromator uses a diffraction grating to disperse broadband light into a spectrum, and it outputs only a narrow portion of the spectrum. This enables the monochromator to produce a narrowband output that can be swept across a wide range of wavelengths. The ability to sweep this narrowband output is important for determining the RSR of a detector because this allows us to measure the change in response of the detector to a known optical power at each wavelength.

The monochromator used in this work was an Acton Research Corporation SP-150, which is shown in Fig. 2. This monochromator uses a halogen light source, which emits broadband light that passes through an entrance slit into the rest of the system. This broadband light is reflected from two mirrors and is incident on a diffraction grating. This diffraction grating disperses the broadband light into a spectrum, and the spectrum is reflected from another mirror. Part of the spectrum passes through the output slit, creating a narrowband output. The diffraction grating is mounted on a rotation stage, which is controlled by a computer to vary the part of the spectrum passing through the output slit. These measurements were made

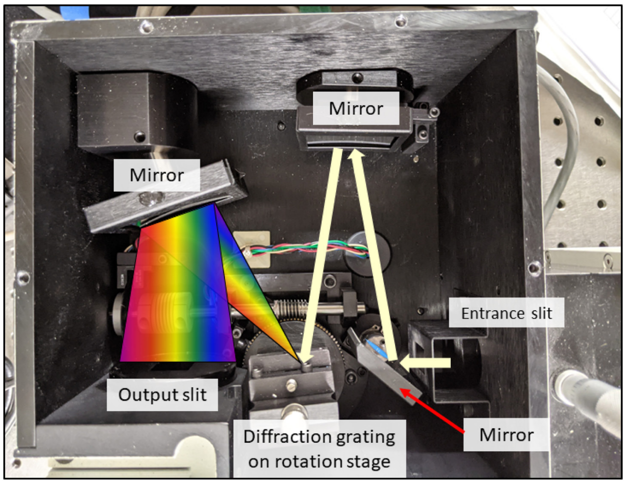

Fig. 2. Top-down view of the inside of the Acton Research Corporation SP-150 monochromator. A halogen light source emits light, which passes through the entrance slit, reflects off two mirrors, and is dispersed by a reflective diffraction grating on a rotation stage. The spectrum reflects from another mirror and a portion of the spectrum passes through the output slit. Photograph provided courtesy of Musaddeque Syed.

using a diffraction grating with 300 grooves per millimeter, an entrance slit width of 2 mm, and an exit slit width of 1 mm.

The polarization of the monochromator output can be attributed to three primary factors. The first is the halogen lamp used as the source; it is well known that lamp filaments can emit partially polarized light, especially when viewed at oblique angles of incidence [24–27]. Next, when light is incident on a mirror, the parallel and perpendicular components (referenced to the plane of incidence) are reflected by different amounts according to the Fresnel coefficients. Thus, the light from the halogen lamp is further polarized by reflections from the three mirrors in the system. Finally, reflection from a diffraction grating also has a polarizing effect that changes as a function of wavelength and incidence angle. As a result, when the diffraction grating is rotated and the incidence angle is changed to control the wavelength passing through the output slit, the polarization state of the output light varies.

3. MONOCHROMATOR OUTPUT POLARIZATION MEASUREMENTS

We began by investigating the monochromator output polarization. It was measured using each DoFP camera and verified using an optical power meter (Thorlabs PM320E) with a custom-built polarizer (Meadowlark Optics Versalight, aluminum wire grid on UV-grade fused silica substrate) mounted on a precision rotation stage (Newport RV160CC). It should be noted that measuring the monochromator output polarization with the camera relies on the assumption that all subpixels have the same RSR. In other words, the flat-field correction for broadband light was applied to account for variation in the responsivity of individual pixels, and we assume that it is valid for illumination by the narrowband monochromator output as it is swept across the range of the detector.

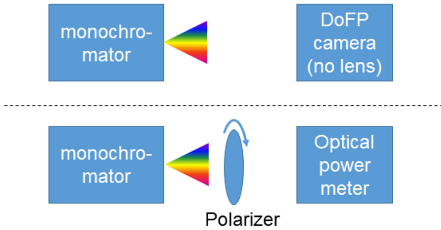

Fig. 3. This setup was used to measure the polarization of the monochromator output: (top) DoFP camera used to measure monochromator polarization; (bottom) wire-grid polarizer and optical power meter measurements to verify monochromator polarization sensitivity.

First, the camera with no lens was placed in front of the monochromator, so the monochromator output was incident directly on the sensor. The monochromator output was swept from 400 to 1000 nm in 2-nm steps, and at each wavelength an image was recorded of the monochromator output. The I_{0°, I_{45°, I_{90°, and I_{135° images were extracted, and a region of interest where the monochromator output was illuminating the sensor was identified. An average value for each of the four irradiances was calculated by taking the mean across all the pixels in the region of interest, and DoLP and AoP were calculated from these values using Eqs. (1)–(5). This was done for both the FLIR and the Lucid cameras. Next, these results were verified by making independent measurements of I_{0°, I_{45°, I_{90°, and I_{135° with a wire-grid polarizer mounted on a precision rotation stage in front of an optical power meter. These verification measurements were only made at wavelengths where the DoFP cameras measured a local maximum or minimum in the DoLP curve. The setup for measuring the polarization with the DoFP camera is shown in the top half of Fig. 3, and the setup for measuring the polarization with a wire-grid polarizer and power meter is shown in the bottom half. The results are shown in Fig. 4. We found that our monochromator has a DoLP that varies significantly as a function of wavelength, swinging from DoLP maxima of greater than 0.7 to minima of less than 0.1. The output was found to be vertically polarized (AoP $= 90^\circ$) over most of the spectral range of the DoFP cameras, but it was horizontally polarized from 508 to 564 nm.

We attribute discrepancies between the measurements from the two cameras and the power meter and polarizer setup primarily to the spatial variation of the monochromator output as a function of wavelength. The spatial variation caused partial detector illumination at some wavelengths, making it difficult to choose an accurate region of interest for all wavelengths. Also, the cameras were placed on a tripod pointing at the monochromator, resulting in a slightly different location relative to the monochromator and therefore illumination by a slightly different part of the monochromator output for each camera. As is shown in the next section, the spatial nonuniformity of the monochromator output caused uncertainty in the measured RSR. An iris was therefore inserted between the monochromator output and the camera to limit the spatial variation of the illumination on the detector. Both cameras were used to repeat the process outlined above for calculating the DoLP and AoP of the monochromator. The results with the iris are shown in

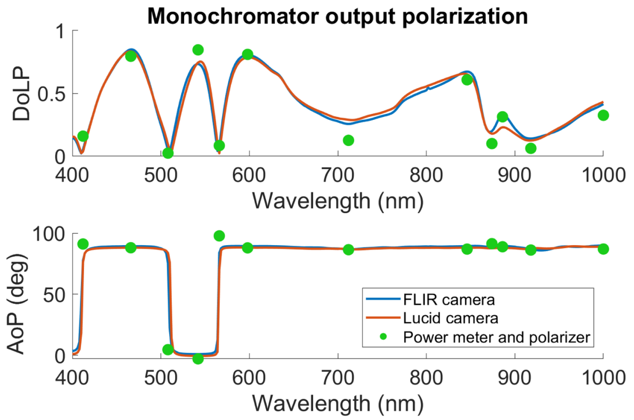

Fig. 4. Polarization state of the full monochromator output as a function of wavelength. Measurements were made with the FLIR camera, the Lucid camera, and an optical power meter and polarizer.

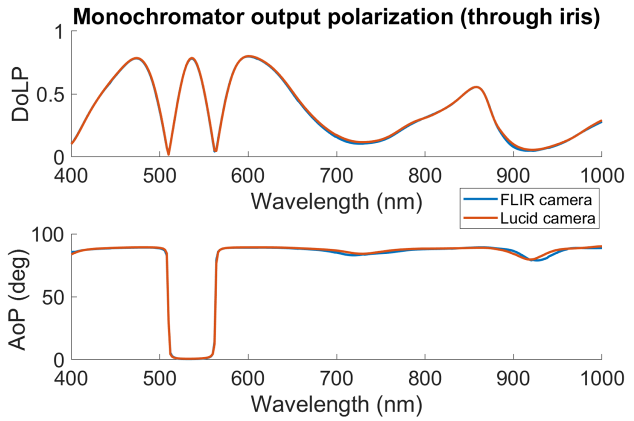

Fig. 5. Polarization state of the monochromator output through an iris as a function of wavelength. Measurements were made with the FLIR camera and the Lucid camera.

Fig. 5. This represents the tunable light source used for the better spectral characterizations shown in the next section.

4. RSR MEASUREMENTS

Typically, an RSR is measured by illuminating a detector with a narrowband source of known output power and sweeping the source across the wavelength range of the detector. However, when the detector and the source both have a nonnegligible state of polarization, the measured RSR will be corrupted with polarization artifacts. In the case of these DoFP polarization cameras, the individual subpixels cannot be characterized with the polarized monochromator. However, at each superpixel, the S_0 Stokes parameter, a polarization-insensitive value, can be calculated. Thus, we can assume that the individual subpixels within a superpixel have the same RSR and characterize the change in S_0 as the monochromator output is swept across the wavelength range of the camera.

To measure the RSR, we first illuminated the camera directly with the monochromator output and recorded an image at each wavelength. Then, we measured the optical power of the monochromator at each wavelength. To obtain the RSR

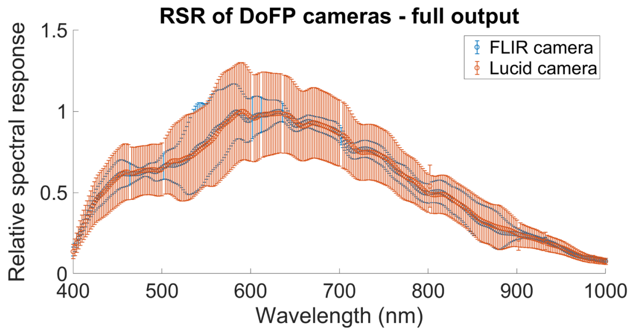

Fig. 6. RSR curve of the FLIR and Lucid cameras, measured with the full monochromator output. The error bars show the standard deviation of the values measured by all the superpixels in the region of interest. One outlier was removed from the FLIR data, and six outliers were removed from the Lucid data.

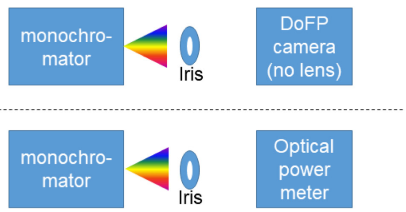

Fig. 7. Setup used to measure RSR of the DoFP camera. Measurements were made with and without the iris shown; the iris is used in our recommended method.

curve, an average S_0 value was found over all the superpixels in a region of interest for each wavelength and was divided by the optical power at the same wavelength. The curve was then normalized to have a maximum value of 1. The RSR measured using illumination by the full monochromator output is shown in Fig. 6. As explained above, the monochromator output was found to have significant spatial variation across its output, and the output changed as a function of wavelength. This caused individual superpixels to be illuminated with a higher or lower optical power, even though all superpixels were normalized by the optical power averaged across the entire output. As a result of the high spatial variation, the signal-to-noise ratio (SNR) of the RSR data, defined as the mean of all superpixels in the region of interest divided by the standard deviation, was low.

The above process was repeated with an iris placed between the monochromator output and the camera to decrease the spatial variation of the illumination. The setup for this measurement is shown in Fig. 7, with the top half showing the setup for recording images with the DoFP camera and the bottom half showing the setup for measuring the optical power of the monochromator output. The setup for the measurement described above was identical, except there was no iris. An example of an image recorded by the DoFP camera with the iris in place is shown in Fig. 8, and the red circle approximately denotes the region of interest used. Without the iris, the region of interest was 50% of the sensor area for the images recorded with the FLIR camera and 80% for the images recorded with the Lucid camera (this difference resulted from the variation in illumination by the monochromator output discussed previously).

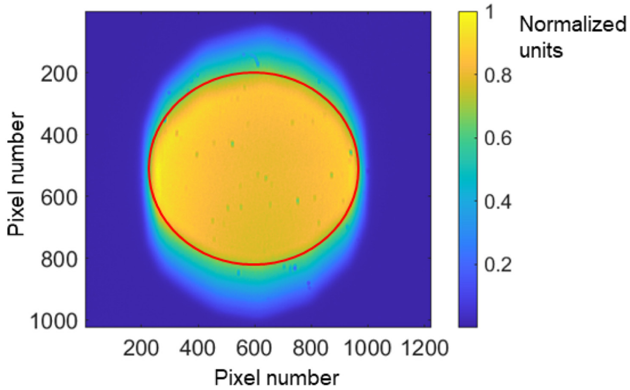

Fig. 8. Example of an image recorded while using an iris to limit the spatial extent of the monochromator output. The red circle denotes the approximate region of interest used in analysis.

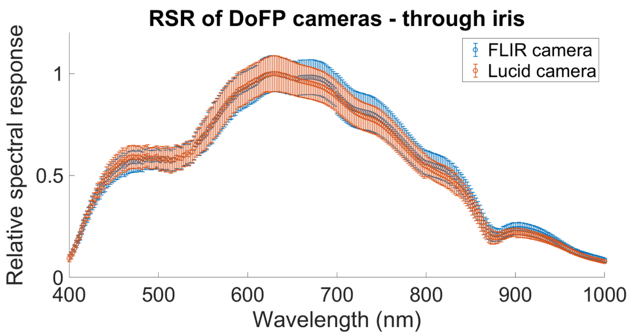

Fig. 9. RSR curve of the FLIR and Lucid cameras, measured with the monochromator output passing through an iris. The error bars show the standard deviation of the values measured by all the superpixels in the region of interest.

The location of the monochromator and the iris were fixed relative to one another, so both cameras and the power meter measured the same part of the monochromator output. The RSR curves measured using the limited monochromator output are shown in Fig. 9. Adding an iris decreased the standard deviation in the measured RSR, smoothed the RSR curves, and improved the degree of similarity between the FLIR and Lucid curves, which was expected, since both cameras use the same sensor. When the iris was added, the wavelength corresponding to maximum responsivity shifted from 632 to 630 nm for the FLIR camera, and from 590 to 630 nm for the Lucid camera. For the FLIR camera, the minimum SNR in the RSR data increased from 2.34 at 878 nm to 5.71 at 870 nm, and for the Lucid camera it increased from 2.09 at 880 nm to 5.40 at 870 nm. The differences are attributed to errors from the spatial variation of the monochromator output and partial detector illumination in the first set of measurements, and the measurements with the iris are accepted as more accurate.

We also repeated the analysis using different equations to calculate S_0. It is possible to calculate S_0 with Eq. (1) or with either of the following:

$$S_0 = I_{45^\circ} + I_{135^\circ}, \tag{6}$$

$$S_0 = \frac{1}{2}(I_{0^\circ} + I_{45^\circ} + I_{90^\circ} + I_{135^\circ}). \tag{7}$$

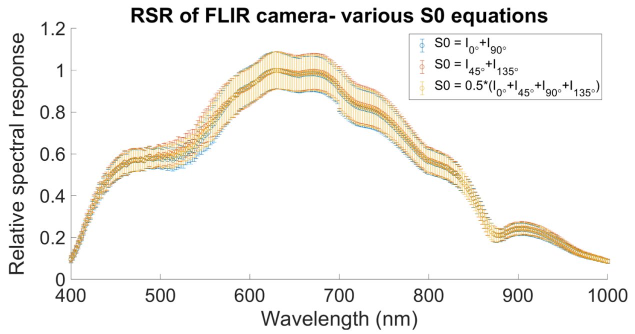

Fig. 10. RSR curve of the FLIR camera, calculated using different equations for S_0. The error bars show the standard deviation of the values measured by all the superpixels in the region of interest.

The RSRs obtained by using Eqs. (1), (6), and (7) are shown in Fig. 10. The curves calculated with Eqs. (1) and (6) vary by a maximum of 0.0465, and the curve calculated with Eq. (7) is the mean of the first two. Choice of an equation for S_0 should depend on how S_0 will be calculated in the user's application.

In summary, the simple method to measure the RSR while avoiding polarization artifacts is described by the following steps:

1. If desired, characterize the polarization state of the source as a function of wavelength as outlined in Section 3.
2. Depending on the spatial variation of the source, insert an iris between the source and the camera. The iris size should be chosen such that there is a region of fairly uniform illumination on the sensor.
3. Illuminate the camera sensor directly with the monochromator output. Perform a wavelength sweep across the spectral range of the camera, and record an image at each wavelength.
4. Replace the camera with an optical power meter, and repeat the wavelength sweep, measuring the optical power of the source at each wavelength.
5. At each wavelength, calculate the S_0 value at each superpixel in a region of interest. S_0 should be calculated using Eqs. (1), (6), or (7), according to the user's application.
6. Average the S_0 values of all superpixels in the region of interest. Divide the average S_0 values by the optical power of the source at the respective wavelength.
7. Normalize the maximum value to 1 to obtain the RSR curve.

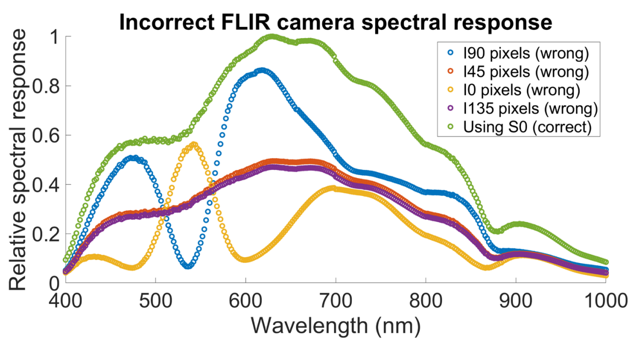

Fig. 11. Incorrect RSR curve of the FLIR camera, calculated for individual polarized subpixels while ignoring the polarization of the monochromator output.

Finally, as an example of the error that would result from neglecting the source polarization, the data were reprocessed in an incorrect way. Instead of calculating S_0 for a superpixel, the values of individual subpixels were extracted to form four images of irradiance at 0°, 45°, 90°, and 135° at each wavelength. In each image, the pixels in the region of interest were averaged, and the averages were plotted as a function of wavelength. The four resulting incorrect curves are plotted with the correct RSR in Fig. 11 to show the extent to which polarization artifacts can corrupt an RSR.

5. DISCUSSIONS AND CONCLUSIONS

The monochromator output was found to be strongly polarized, with a polarization state that varies as a function of wavelength. Specifically, the polarization varies as the angle of the diffraction grating within the monochromator is changed. The DoLP was found to swing from maxima above 0.7 to minima below 0.1, and the AoP was found to be vertical over most of the spectral range but horizontal from 508 to 564 nm. We previously identified three mechanisms by which the output could become polarized: the polarization of the lamp filament, reflections from the mirrors, and reflection from the diffraction grating. The reflection from the diffraction grating is likely to be the dominant cause of the strong polarization response that we observe, since the polarization due to the mirrors or lamp filament are expected to be much smaller and spectrally flatter.

We presented a simple method of obtaining the RSR of a DoFP polarization imager by direct illumination from a monochromator output. No additional optical components are required besides a monochromator, an optical power meter, and an iris. In general, polarization artifacts are present in the RSR when a polarized source is used to perform a spectral characterization of a polarized imager, but this method of characterizing the S_0 Stokes parameter avoids this problem. It was also shown that when the polarization of the source was ignored, the resulting incorrect spectral response curve had extremely large errors. Therefore, it is necessary to account for source polarization when characterizing a polarized imager. While it may be possible to do so using an integrating sphere or an achromatic wave plate, the method presented here is simple and requires no additional optical components. Using this method, we measured the RSR of two DoFP cameras. The wavelength with the highest responsivity was 630 nm for both the FLIR camera and the Lucid camera. Also, the spatial variation of the detector illumination was decreased by passing the monochromator output through an iris. This was shown to increase the SNR of the RSR data, from a minimum of 2.34 to 5.71 for the FLIR camera data, and from a minimum of 2.09 to 5.40 for the Lucid camera data. Finally, the RSRs obtained for the FLIR and Lucid cameras were found to be very similar. The cameras are made by different manufacturers, but both use Sony's recently released polarization sensor. Thus, the two cameras are expected to have similar RSRs, and the similarity between the two RSRs that we measured supports the validity of this method. We expect that this method of characterizing DoFP cameras will become increasingly useful as recent DoFP sensor technology improvements enable an increasing number of applications for these cameras.

Funding. Air Force Research Laboratory (FA8650-16-C-1954); National Science Foundation (OIA-1757351); Montana Space Grant Consortium.

Acknowledgment. We acknowledge Musaddeque Syed for his help with initial measurements and photograph of the monochromator interior. An early version of this work was published in the SPIE Proceedings volume for the Polarization Science and Remote Sensing X Conference {Ref. [21]}. E. Venkatesulu acknowledges the Montana Space Grant Consortium for fellowship funding. This research was conducted with partial support from the National Science Foundation EPSCoR Program through Cooperative Agreement and partial support from the U.S. Air Force Research Laboratory via a subcontract from S2 Corp. with a fundamental research exemption.

Disclosures. The authors declare no conflicts of interest.

Data availability. Data underlying the results presented in this paper are available in Ref. [28].

REFERENCES

1. J. S. Tyo, D. L. Goldstein, D. B. Chenault, and J. A. Shaw, "Review of passive imaging polarimetry for remote sensing applications," Appl. Opt. **45**, 5453–5469 (2006).
2. Y. Maruyama, T. Terada, T. Yamazaki, Y. Uesaka, M. Nakamura, Y. Matoba, K. Komori, Y. Ohba, S. Arakawa, Y. Hirasaw, Y. Kondo, J. Murayama, K. Akiyama, Y. Oike, S. Sato, and T. Ezaki, "3.2-MP back-illuminated polarization image sensor with four-directional air-gap wire grid and 2.5-μm pixels," IEEE Trans. Electron Dev. **65**, 2544–2551 (2018).
3. A. Corrons and E. F. Zalewski, "Detector spectral response from 350 to 1200 nm using a monochromator based spectral comparator," Technical Note 988 (National Bureau of Standards, 1978).
4. L.-P. Boivin, "Study of bandwidth effects in monochromator-based spectral responsivity measurements," Appl. Opt. **41**, 1929–1935 (2002).
5. J. A. Barsi, K. Lee, G. Kvaran, B. L. Markham, and J. A. Pedelty, "The spectral response of the Landsat-8 operational land imager," Remote Sens. **6**, 10232–10251 (2014).
6. K. Bücher and A. Schönecker, "Spectral response measurements of multi-junction solar cells with a grating monochromator and a Fourier spectrometer," in *10th European Commission Photovoltaic Solar Energy Conference* (2017), pp. 107–110.
7. T. Hashimoto, L. M. Dahl, S. A. Laurie, and J. A. Shaw, "Camera characterization for all-sky polarization measurements during the 2017 solar eclipse," Proc. SPIE **10407**, 1040706 (2017).
8. O. Gravrand, J. Wlassow, and L. Bonnefond, "A calibration method for the measurement of IR detector spectral responses using a FTIR spectrometer equipped with a DTGS reference cell," Proc. SPIE **9154**, 91542O (2014).
9. S. W. Brown, G. P. Eppeldauer, and K. R. Lykke, "Facility for spectral irradiance and radiance responsivity calibrations using uniform sources," Appl. Opt. **45**, 8218–8237 (2006).
10. M. Schuster, S. Nevas, A. Sperling, and S. Völker, "Spectral calibration of radiometric detectors using tunable laser sources," Appl. Opt. **51**, 1950–1961 (2012).
11. K. Mahmoud, S. Park, S.-N. Park, and D.-H. Lee, "Measurement of normalized spectral responsivity of digital imaging devices by using a LED-based tunable uniform source," Appl. Opt. **52**, 1263–1271 (2013).
12. O. Furxhi, D. Haefner, and S. Burks, "Instrument for the measurement of normalized spectral response of cameras in the thermal bands," Proc. SPIE **10625**, 1062503 (2018).
13. M. E. Toivonen and A. Klami, "Practical camera sensor spectral response and uncertainty estimation," J. Imaging **6**, 79 (2020).
14. J. A. Shaw, "The effect of instrument polarization sensitivity on sea surface remote sensing with infrared spectroradiometers," J. Atmos. Ocean. Technol. **19**, 820–827 (2002).
15. J. Young, E. Knight, and C. Merrow, "MODIS polarization performance and anomalous four-cycle polarization phenomenon," Proc. SPIE **3439**, 246–256 (1998).
16. J.-Q. Sun and X. Xiong, "MODIS polarization-sensitivity analysis," IEEE Trans. Geosci. Remote Sens. **45**, 2875–2885 (2007).

17. J. K. Taylor, H. E. Revercomb, and D. C. Tobin, "An analysis and correction of polarization induced calibration errors for the cross-track infrared sounder (CrIS) sensor," in *Light, Energy and the Environment 2018 (E2, FTS, HISE, SOLAR, SSL)* (Optical Society of America, 2018), paper FW2B.3.
18. A. Angal, X. Geng, X. Xiong, K. A. Twedt, A. Wu, D. O. Link, and E. Aldoretta, "On-orbit calibration of terra MODIS VIS bands using polarization-corrected desert observations," IEEE Trans. Geosci. Remote Sens. **58**, 5428–5439 (2020).
19. T. York and V. Gruev, "Characterization of a visible spectrum division-of-focal-plane polarimeter," Appl. Opt. **51**, 5392–5400 (2012).
20. M. W. Kudenov, M. E. Lowerstern, J. M. Craven, and C. F. LaCasse, "Field deployable pushbroom hyperspectral imaging polarimeter," Opt. Eng. **56**, 103107 (2017).
21. E. Venkatesulu, M. A. Syed, and J. A. Shaw, "Polarimetric characterization of a monochromator to measure the spectral response of a pixelated polarization imager," Proc. SPIE **11833**, 118330G (2021).
22. T. Yamazaki, Y. Maruyama, Y. Uesaka, M. Nakamura, Y. Matoba, T. Terada, K. Komori, Y. Ohba, S. Arakawa, Y. Hirasawa, Y. Kondo, J. Murayama, K. Akiyama, Y. Oike, S. Sato, and T. Ezaki, "Four-directional pixel-wise polarization CMOS image sensor using air-gap wire grid on 2.5-μm back-illuminated pixels," in *International Electron Devices Meeting* (IEEE, 2016), pp. 220–223.
23. S. C. McClain, C. L. Bartlett, J. L. Pezzaniti, and R. A. Chipman, "Depolarization measurements of an integrating sphere," Appl. Opt. **34**, 152–154 (1995).
24. O. Sandus, "A review of emission polarization," Appl. Opt. **4**, 1634–1642 (1965).
25. D. Spooner, "Polarization pattern of a high intensity incandescent lamp," Appl. Opt. **11**, 2984–2986 (1972).
26. R. K. Kostuk, "Polarization characteristics of a 100-W FEL-type filament lamp," Appl. Opt. **20**, 2181–2182 (1981).
27. K. J. Voss and L. B. da Costa, "Polarization properties of FEL lamps as applied to radiometric calibration," Appl. Opt. **55**, 8829–8832 (2016).
28. E. Venkatesulu, "DoFP polarization camera spectral response," GitLab, 2022, https://gitlab.com/orsl/dofp-polarization-camera-spectral-response.